

Electronic Supporting Information

Unexpected photo-induced oxidative cyclization and luminescence switching in molecular aggregates of two acylhydrazone-based Ir(III) complexes

Xin-Tong Lv,^a Xiao-Dong Liu,^a Zhiping Zhou^c and Deng-Ke Cao^{*a,b}

^aState Key Laboratory of Coordination Chemistry, Coordination Chemistry Institute, School of Chemistry and Chemical Engineering, Nanjing University, Nanjing 210093, P. R. China.

^bEngineering Research Center of Photoresist Materials, Ministry of Education, P. R. China.

^cSchool of Chemistry and Chemical Engineering, Nanjing University, Nanjing 210093, P. R. China.

Table of Contents

1.1 Materials and methods.....	S2
1.2 Syntheses.....	S2
1.3 Single-crystal X-ray crystallography.....	S4
1.4 UV-vis absorption spectra.....	S4
1.5 References.....	S5
1.6 Supporting Scheme.....	S6
1.7 Supporting Tables.....	S6
1.8 Supporting Figures.....	S8

1.1 Materials and methods

Compounds $\text{Ir}_2(\text{ppy})_4\text{Cl}_2$, $\text{Ir}_2(\text{dfppy})_4\text{Cl}_2$, $\text{N}'\text{-}((4'\text{-methyl-[2,2'-bipyridin]-4-yl)methylene)benzohydrazide$ (mbpymbh) and $[\text{Ir}(\text{ppy})_2(\text{mbpymbh})]\text{PF}_6$ (**1**) were prepared according to the literatures [ppyH = 2-phenyl-pyridine and dfppyH = 2-(2,4-difluorophenyl)-pyridine].^{S1,S2} All other reagents were commercially available and used without further purification. Elemental analyses were performed on a Perkin Elmer 240C elemental analyzer. The ^1H NMR spectra were recorded at room temperature with a 400 MHz BRUKER spectrometer. The electrospray (ES) mass spectra of complexes were measured using thermofisher Q exactive. MALDI-TOF spectrum of mbpymbh was carried out using Bruker Ultraflex extreme UV-vis absorption spectra were measured on a Cary 100 spectrophotometer. The transmission electron microscopy (TEM) study was performed using a JEM-2100 electron microscope. Luminescence spectra were measured using a Hitachi F-4600 fluorescence spectrometer. The luminescence lifetimes were measured at room temperature on a HORIBA FL-3 Spectrofluorometer with a 370 nm LED pulsed from a NanoLED resource. The luminescence quantum yields of complexes **1** and **2** in solution were measured by a relative method by comparison with a standard, a solution of quinine sulfate in 0.5 M H_2SO_4 ($\Phi = 54.6\%$, $\lambda_{\text{ex}} = 366$ nm).^{S3} The Electron paramagnetic resonance (EPR) data were collected using a Bruker EMX plus spectrometer at room temperature.

1.2 Syntheses

Synthesis of $[\text{Ir}(\text{ppy})_2(\text{mbpymbh})]\text{PF}_6$ (**1**)

Under the protection of Ar, a mixture of $\text{Ir}_2(\text{ppy})_4\text{Cl}_2$ (0.1608 mg, 0.15 mmol) mbpymbh (0.0950 g, 0.3 mmol), CH_2Cl_2 (15 mL) and CH_3OH (15 mL) was heated at 50 °C for 4 hours. After evaporation under vacuum, the resultant solid was dissolved in a mixture of CH_2Cl_2 (30 mL) and saturated KPF_6 aqueous solution (20 mL). This mixture was vigorously stirred at room temperature for two hours, and then extracted with CH_2Cl_2 (30 mL) twice. The combined CH_2Cl_2 solution was dried with MgSO_4 , filtered, and evaporated. The resultant residue was purified through silica column chromatography using a $\text{CH}_3\text{OH}-\text{CH}_2\text{Cl}_2$ (v/v = 2/100) solution, obtaining a red solid with a yield of 212 mg (74% based on $\text{Ir}_2(\text{ppy})_4\text{Cl}_2$). Anal. calcd for $\text{C}_{41}\text{H}_{32}\text{N}_6\text{OF}_6\text{PIr}$: C, 51.19%; H, 3.35%; N, 8.74%. Found: C, 51.27%; H, 3.51%; N, 8.80%. ^1H NMR (400 MHz, CDCl_3): 2.60 (s, 3H), 6.27-6.33 (m, 2H), 6.90-7.07 (m, 6H), 7.21 (d, $J=5.2$ Hz, 1H), 7.44-7.54 (m, 5H), 7.68-7.97 (m, 11H), 8.52(s, 1H), 8.59 (s, 1H), 8.85 (s, 1H), 10.63 (s, 1H). ES mass spectra: a peak at 817.22 from $[\text{Ir}(\text{ppy})_2(\text{mbpymbh})]^+$ cation.

Synthesis of [Ir(dfppy)₂(mbpymbh)]PF₆ (**2**)

Complex **2** was prepared by the same method as **1**, using Ir₂(dfppy)₄Cl₂ instead of Ir₂(ppy)₄Cl₂. Its crude product was purified through silica column chromatography using a CH₃OH-CH₂Cl₂ (v/v = 1-2/100) solution, obtaining an orange solid with a yield of 214 mg (69% based on Ir₂(dfppy)₄Cl₂). Anal. calcd for C₄₁H₂₈N₆OF₁₀PIr: C, 47.63%; H, 2.73%; N, 8.13%. Found: C, 47.75%; H, 2.94%; N, 8.22%. ¹H NMR (400 MHz, CDCl₃): 2.64 (s, 3H), 5.66-5.71 (m, 2H), 6.55-6.63 (m, 2H), 7.04-7.11 (m, 2H), 7.28 (d, J=6.0 Hz, 1H), 7.45-7.55 (m, 5H), 7.77-7.97 (m, 7H), 8.33 (t, J=8.6Hz, 2H), 8.52 (s, 1H), 8.60 (s, 1H), 8.84 (s, 1H), 10.58 (s, 1H). ES mass spectra: a peak at 889.19 from [Ir(dfppy)₂(mbpymbh)]⁺ cation.

Synthesis of complex of **1-O**

A mixture of complex **1** (0.015 mmol, 14.5 mg) and CH₃CN-H₂O (v/v = 1/9, 150 mL) was stirred and irradiated for 90 minutes with a 365 nm light. After evaporation under vacuum, the resultant residue was purified through silica-gel plate using a CH₃OH-CH₂Cl₂ (v/v = 2/100) solution, obtaining an orange solid with a yield of 8 mg (56 % based on complex **1**). Anal. calcd for C₄₁H₃₀N₆OF₆PIr: C, 51.30%; H, 3.15%; N, 8.76%. Found: C, 51.42%; H, 3.30%; N, 8.89%. ¹H NMR (400 MHz, CDCl₃): 2.69 (s, 3H), 6.28-6.33 (m, 2H), 6.91-6.97 (m, 2H), 7.03-7.08 (m, 4H), 7.35 (m, 1H), 7.52-7.59 (m, 4H), 7.63 (d, J=4.0 Hz, 1H), 7.69 (d, J = 8.0 Hz, 2H), 7.74-7.81 (m, 3H), 7.91 (d, J = 8.0 Hz, 2H), 8.11-8.16 (m, 2H) 8.29-8.32 (m, 2H), 8.65 (s, 1H), 9.12 (s, 1H). ES mass spectra: a peak at 815.21 from complex cation in **1-O**.

Synthesis of complex of **2-O**

A mixture of complex **2** (0.015 mmol, 15.5 mg) and CH₃CN-H₂O (v/v = 1/9, 150 mL) was stirred and irradiated for 40 minutes with a 365 nm light. After evaporation under vacuum, the resultant residue was purified through silica-gel plate using a CH₃OH-CH₂Cl₂ (v/v = 1-2/100) solution, obtaining a yellow solid with a yield of 8.5 mg (54.9% based on complex **2**). Anal. calcd for C₄₁H₂₆N₆OF₁₀PIr: C, 47.72%; H, 2.54%; N, 8.14%. Found: C, 47.85%; H, 2.79%; N, 8.30%. ¹H NMR (400 MHz, CDCl₃): 2.71 (s, 3H), 5.67-5.73 (m, 2H), 6.56-6.63 (m, 2H), 7.09-7.15 (m, 2H), 7.35 (d, J = 6.0 Hz, 1H), 7.52-7.65 (m, 5H), 7.79-7.84 (m, 3H), 8.12 (d, J = 8.0 Hz, 1H), 8.21 (d, J = 4.0 Hz, 1H), 8.28-8.34 (m, 4H), 8.68 (s, 1H), 9.14 (s, 1H). Electrospray (ES) mass spectra: a peak at 887.17 from complex cation in **2-O**.

1.3 Single-crystal X-ray crystallography

The CH₃OH-CH₂Cl₂ solutions of **1-O** and **2-O** were allowed to slowly evaporate, obtaining orange needlelike single crystals of **1-O**, and yellow needlelike single crystals of **2-O**. Single crystals with dimensions 0.16 × 0.13 × 0.12 mm³ for **1-O** and 0.16 × 0.12 × 0.11 mm³ for **2-O** were used for structural determination on a Bruke D8 Venture diffractometer ($\lambda_{\text{GaK}\alpha} = 1.34139 \text{ \AA}$) at 193 K. A hemisphere of data was collected in the θ range 2.42 to 53.89° for **1-O** and 2.70 to 53.90° for **2-O** using a narrow-frame method with scan widths of 0.90° in ω and an exposure time of 10 s per frame. The numbers of observed and unique reflections are 24431 and 6517 ($R_{\text{int}} = 0.0469$) for **1-O**, 59802 and 6913 ($R_{\text{int}} = 0.0339$) for **2-O**, respectively. The data were integrated using the Siemens *SAINTE* program,^{S3} with the intensities corrected for Lorentz factor, polarization, air absorption, and absorption due to variation in the path length through the detector faceplate. Multi-scan absorption corrections were applied. The structures were solved by direct methods and refined on F^2 by full matrix least squares using *SHELXTL*.^{S4,S5} All the non-hydrogen atoms were located from the Fourier maps, and were refined anisotropically. All H atoms were refined isotropically, with the isotropic vibration parameters related to the non-H atom to which they are bonded. It should be noted that the PF₆⁻ anion in the molecular structure of **2-O** was disorder refinement, by using PART, SADI DFIX and DELU. The crystallographic data for complexes **1-O** and **2-O** are listed in Table S1, and selected bond lengths and angles are given in Tables S2 and S3. CCDC 2403734 and 2403735 contain the supplementary crystallographic data of **1-O** and **2-O**, which can be obtained free of charge from the Cambridge Crystallographic Data Centre via www.ccdc.cam.ac.uk/data_request/cif.

1.4 UV-vis absorption spectra

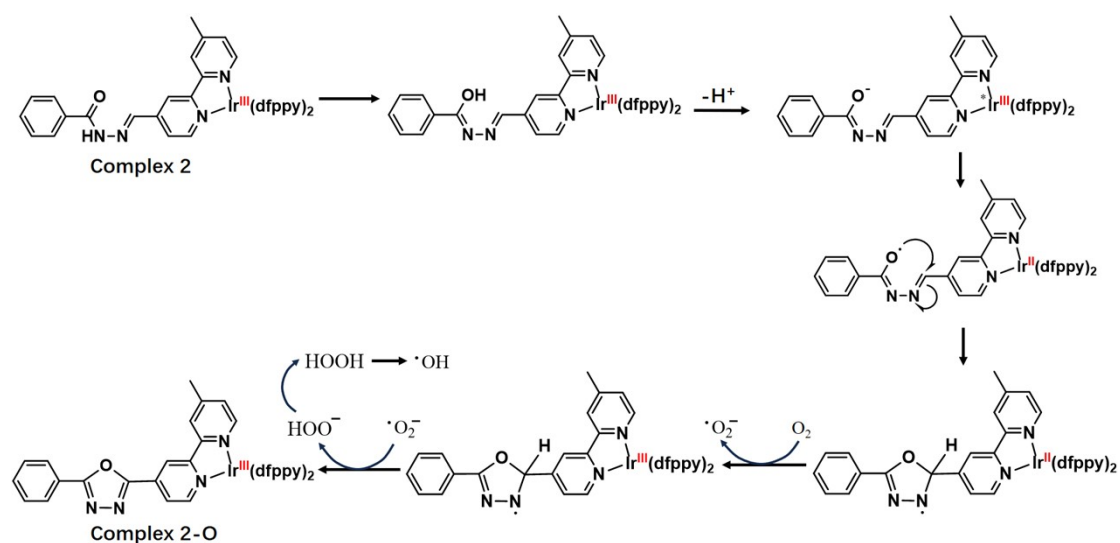
The UV-vis absorption spectra of complexes **1**, **2**, **1-O** and **2-O**, and the related ligands mbpymbh, ppyH and dfppyH were measured in CH₂Cl₂ at room temperature (Table S4, Figs. S9 and S10). The four complexes show high-energy absorption bands at 258 and 305 nm for **1**, 253 and 315 nm for **2**, 257 and 306 nm for **1-O**, and 249 and 313 nm for **2-O**. These bands can be assigned to spin-allowed ligand-centered (¹LC) transitions of ligands mbpymbh and ppy⁻/dfppy⁻, which can be confirmed by the absorption bands of these ligands (246 and 274 nm for ppyH, 237 and 271 nm for dfppyH, and 245 and 290 nm for mbpymbh). The low-energy absorption bands in the

range 350-400 nm in the four complexes are likely to be a combination of spin-allowed metal-to-ligand charge transfer (¹MLCT) and ligand-centered (¹LC) transitions, because of the high extinction coefficients: $\epsilon = 1.16 \times 10^4 \text{ M}^{-1} \text{ cm}^{-1}$ for the band at 362 nm in **1**, $1.83 \times 10^4 \text{ M}^{-1} \text{ cm}^{-1}$ for the band at 355 nm in **2**, $1.00 \times 10^4 \text{ M}^{-1} \text{ cm}^{-1}$ for the band at 369 nm in **1-O**, and $1.23 \times 10^4 \text{ M}^{-1} \text{ cm}^{-1}$ for the band at 359 nm in **2-O**. In addition, complexes **1**, **2**, **1-O** and **2-O** also show weak absorption tails towards to 559 nm for **1**, 517 nm for **2**, 565 nm for **1-O**, and 529 nm for **2-O**, which can be attributed to ³MLCT absorptions.^{S6} Compared to **1** and **2**, their corresponding photoproducts **1-O** and **2-O** reveal clearly red-shifted low-energy absorption bands and absorption tails. This can be due to photo-induced structural transition from acylhydrazone units in **1** and **2** to 1,3,4-oxadiazole units in **1-O** and **2-O** (Scheme 1: transition from 1f to 1g).

1.5 References

- S1 T.-B. Gao, Z.-Z. Qu, Z. Tang and D.-K. Cao, Cyclometalated Ir(III) complexes incorporating a photoactive anthracene-based ligand: syntheses, crystal structures and luminescence switching by light irradiation, *Dalton Trans.* 2017, **46**, 15443–15450.
- S2 N. Zhao, Y.-H. Wu, J. Luo, L.-X. Shi, Z.-N. Chen, Aggregation-Induced Phosphorescence of Iridium(III) Complexes with 2,2'-Bipyridine-Acylhydrazone and Their Highly Selective Recognition to Cu²⁺, *Analyst*, **2013**, *138*, 894–900.
- S3 SAINT, *Program for Data Extraction and Reduction*, Siemens Analytical X-ray Instruments, Madison, WI, 1994–1996.
- S4 SHELXTL, *Reference Manual*, version 5.0, Siemens Industrial Automation, Analytical Instruments, Madison, WI, 1997.
- S5 G. M. Sheldrick, *Acta Crystallogr., Sect. A: Fundam. Crystallogr.* **2008**, *64*, 112–122.
- S6 (a) J. N. Demas and G. A. Crosby, The Measurement of Photoluminescence Quantum Yields, *J. Phys. Chem.* **1971**, *75*, 991-1024; (b) A. M. Brouwer, Standards for Photoluminescence Quantum Yield Measurements in Solution, *Pure Appl. Chem.* **2011**, *83*, 2213-2228.

1.6 Supporting Scheme



Scheme S1 Possible mechanism for photo-induced oxidative cyclization in complex **2** in a CH₃CN-H₂O (v/v = 1/9) mixed solvent.

1.7 Supporting Tables

Table S1 Crystallographic data and refinement of **1-O** and **2-O**.

Formula	C ₄₁ H ₃₂ F ₆ IrN ₆ OP	C ₄₁ H ₂₆ F ₁₀ IrN ₆ OP
<i>M</i>	961.89	1031.85
Crystal system	Triclinic	Monoclinic
Space group	<i>P</i> $\bar{1}$	<i>P</i> 2 ₁ / <i>c</i>
<i>T</i> /K	193(2)	193(2)
<i>a</i> /Å	9.5465(18)	14.2171(14)
<i>b</i> /Å	12.491(2)	14.3986(14)
<i>c</i> /Å	16.051(3)	18.5127(17)
α	85.478(5)	90
β /°	82.505(5)	90.388(3)
γ	75.590(5)	90
<i>V</i> /Å ³	1835.8(6)	3789.6(6)
<i>Z</i>	2	4
<i>D_c</i> /g cm ⁻³	1.740	1.809
<i>F</i> (000)	948	2016
GooF on <i>F</i> ²	1.061	1.052
<i>R</i> ₁ , <i>wR</i> ₂ [<i>I</i> > 2σ(<i>I</i>)] ^a	0.0343, 0.0902	0.0273, 0.0745
<i>R</i> ₁ , <i>wR</i> ₂ (all data) ^a	0.0371, 0.0945	0.0307, 0.0764
(Δρ) _{max} ,	1.000, -1.308	1.455, -0.750
(Δρ) _{min} (e Å ⁻³)		

^a*R*₁ = Σ||*F*_o - |*F*_c|| / Σ|*F*_o|. *wR*₂ = [Σ*w*(*F*_o² - *F*_c²)² / Σ*w*(*F*_o²)²]^{1/2}.

Table S2 Selected bond lengths (Å) and bond angles (°) of **1-O**.

Ir1-N1	2.144(4)	N3-C11	1.285(6)
Ir1-N5	2.054(4)	N4-C12	1.280(8)
Ir1-C20	2.016(5)	O1-C12	1.375(6)
Ir1-N2	2.140(4)	N3-N4	1.402(7)
Ir1-N6	2.054(4)	O1-C11	1.339(6)
Ir1-C31	1.994(5)		
N2-Ir1-N1	75.78(14)	N5-Ir1-N1	87.89(14)
N6-Ir1-N1	97.03(16)	C20-Ir1-N1	100.30(16)
C31-Ir1-N1	170.78(16)	N5-Ir1-N2	98.80(15)
N6-Ir1-N2	87.35(15)	C20-Ir1-N2	176.05(15)
C31-Ir1-N2	95.14(16)	N6-Ir1-N5	172.94(15)
C20-Ir1-N5	80.45(18)	C31-Ir1-N5	95.2(2)
C20-Ir1-N6	93.65(19)	C31-Ir1-N6	80.7(2)
C31-Ir1-C20	88.80(18)		

Table S3 Selected bond lengths (Å) and bond angles (°) of **2-O**.

Ir1-N1	2.135(3)	N3-C11	1.285(5)
Ir1-N5	2.052(3)	N4-C12	1.291(5)
Ir1-C20	2.018(4)	O1-C12	1.375(4)
Ir1-N2	2.131(3)	N3-N4	1.411(5)
Ir1-N6	2.033(3)	O1-C11	1.358(4)
Ir1-C31	2.015(3)		
N2-Ir1-N1	76.23(11)	N5-Ir1-N1	86.95(11)
N6-Ir1-N1	95.83(12)	C20-Ir1-N1	99.76(12)
C31-Ir1-N1	173.88(12)	N5-Ir1-N2	97.62(12)
N6-Ir1-N2	86.78(12)	C20-Ir1-N2	175.82(12)
C31-Ir1-N2	98.75(12)	N6-Ir1-N5	175.27(12)
C20-Ir1-N5	80.87(14)	C31-Ir1-N5	97.27(13)
C20-Ir1-N6	94.86(15)	C31-Ir1-N6	80.26(14)
C31-Ir1-C20	85.32(13)		

Table S4 The UV absorption bands of complexes **1**, **2**, **1-O** and **2-O**, and ligands mbpymbh, ppyH and dfppyH in CH₂Cl₂ at room temperature.

compound	λ_{abs} (nm)
1	258, 305, 362 and a tail to 559 nm
2	253, 315, 355, and a tail to 517 nm
1-O	257, 306, 369 and a tail to 565 nm
2-O	249, 313, 359 and a tail to 529 nm
mbpymbh	245, 290 nm
ppyH	246, 274 nm
dfppyH	237, 271 nm

1.8 Supporting Figures

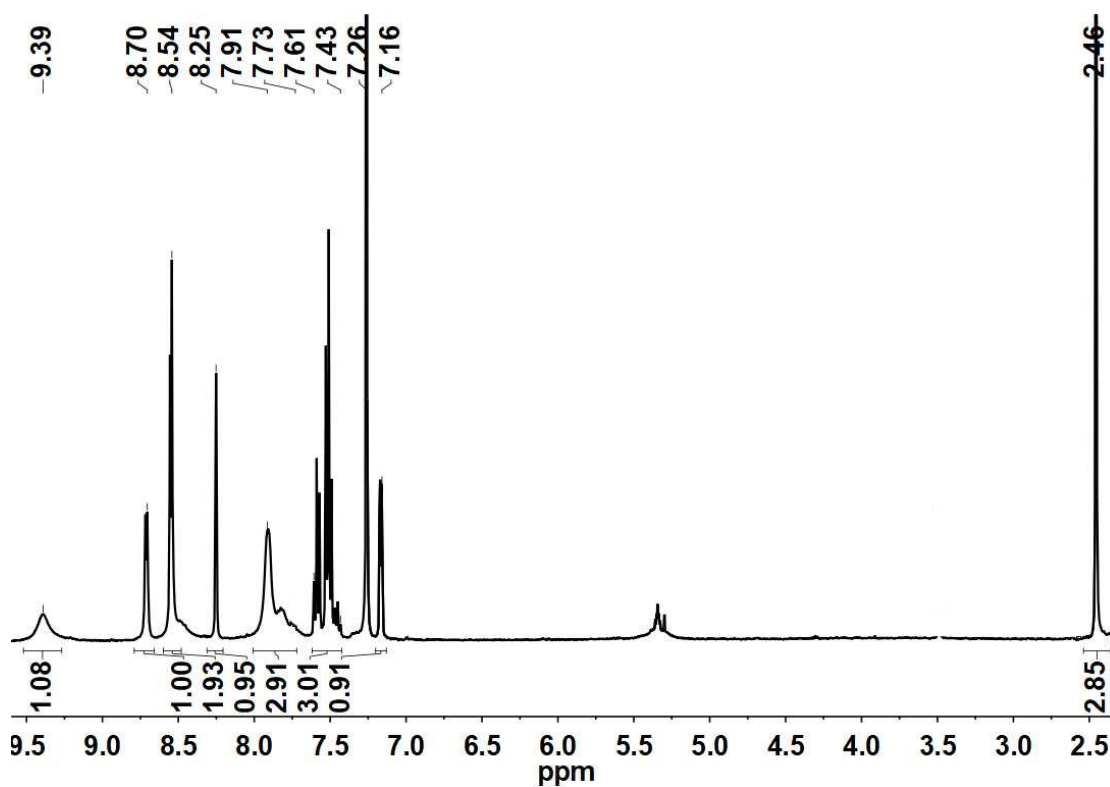


Fig. S1 The ¹H NMR of mbpymbh (400 MHz, CDCl₃).

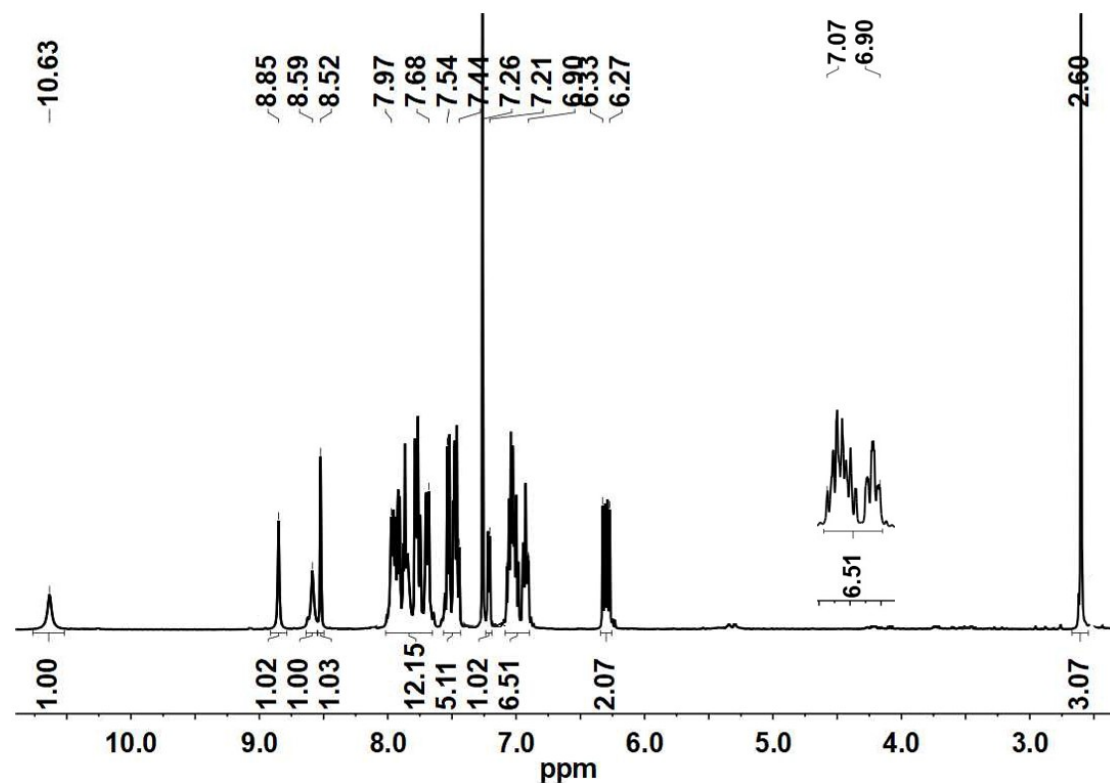


Fig. S2 The ¹H NMR of complex 1 (400 MHz, CDCl₃; inset: the peak in range 6.90-7.07 ppm).

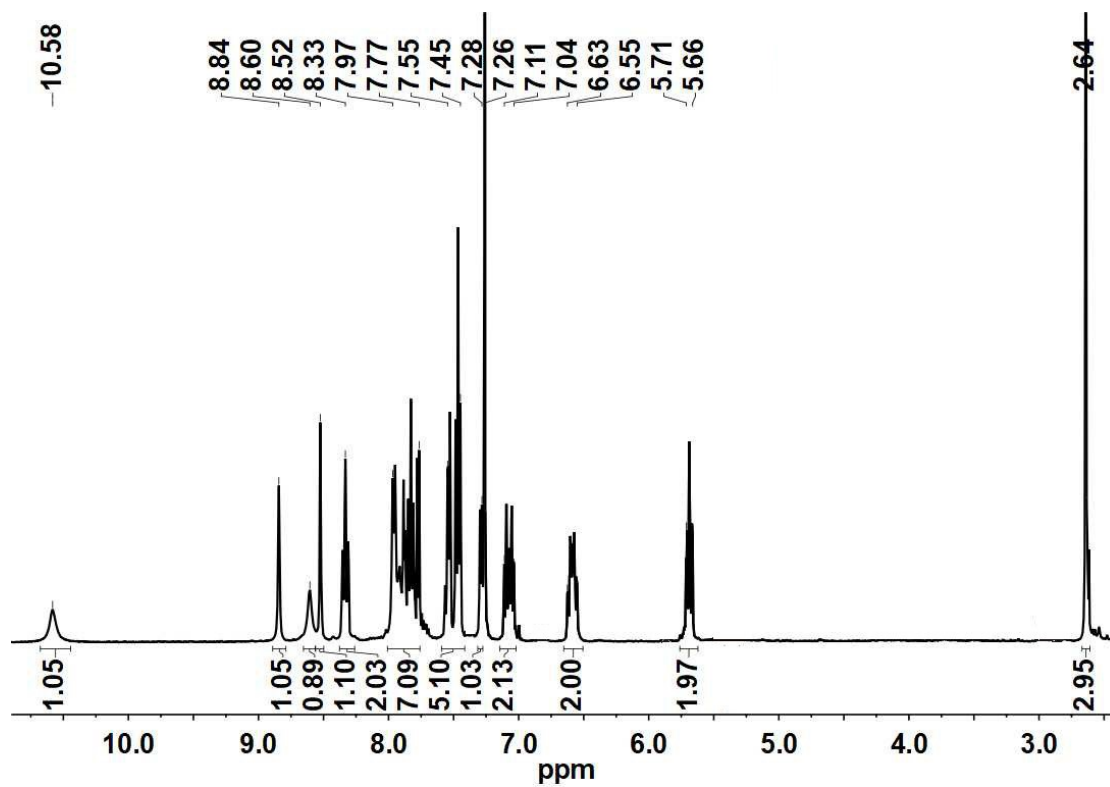


Fig. S3 The ^1H NMR of complex **2** (400 MHz, CDCl_3).

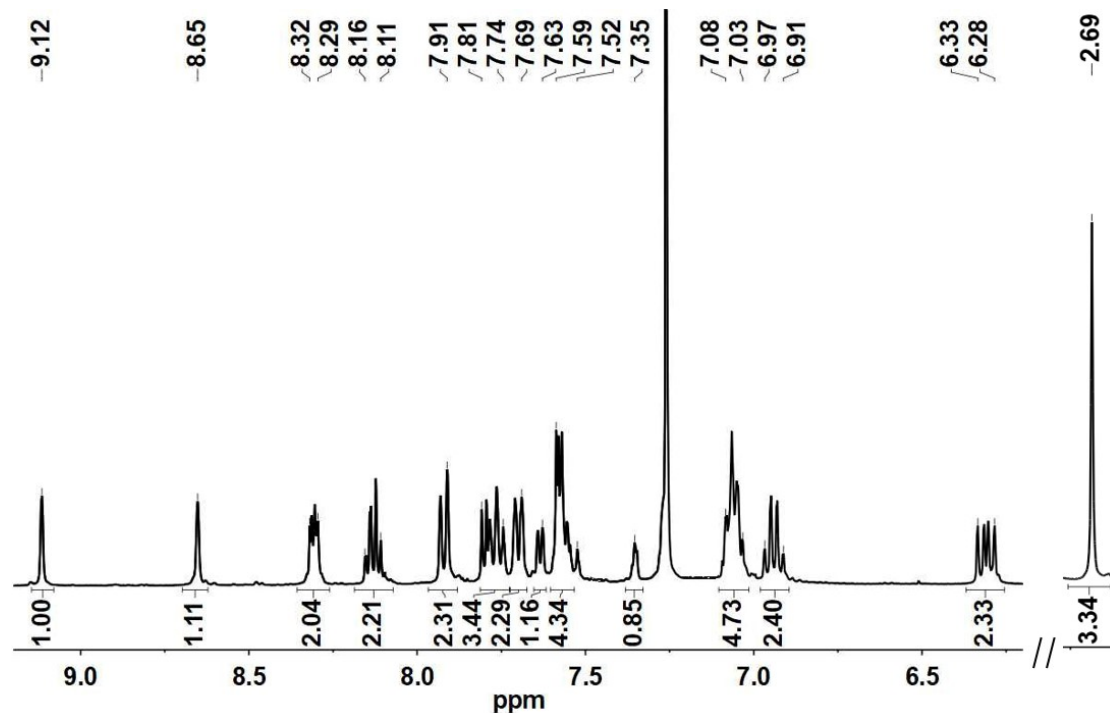


Fig. S4 The ^1H NMR of complex **1-O** (400 MHz, CDCl_3).

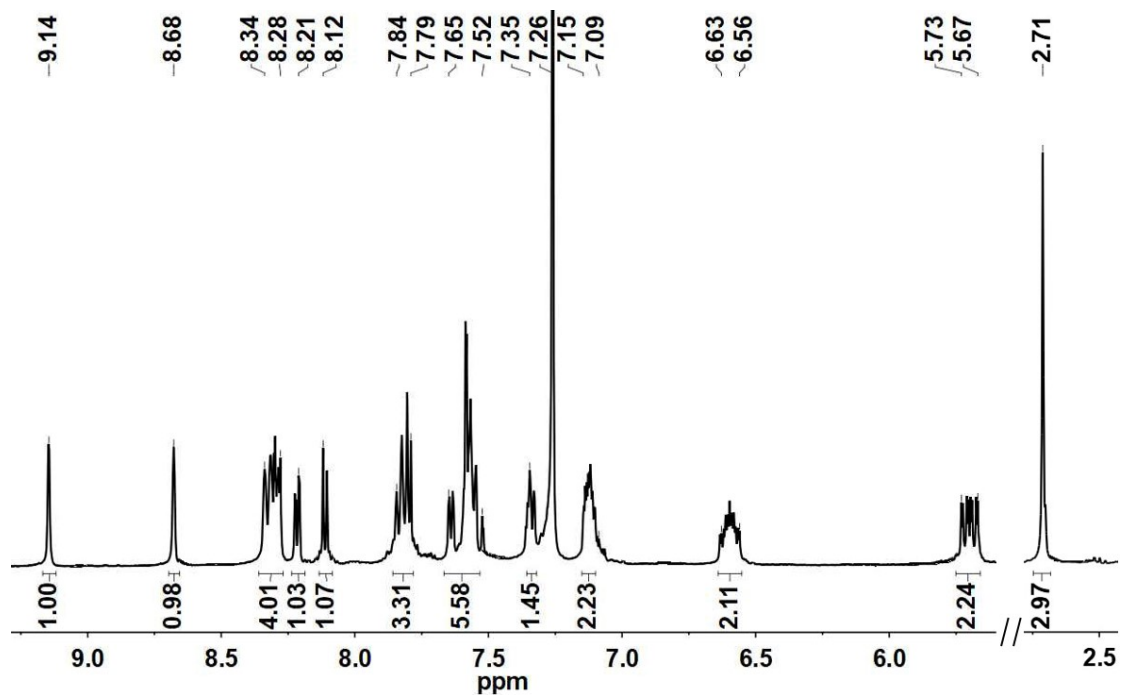


Fig. S5 The ^1H NMR of complex **2-O** (400 MHz, CDCl_3).

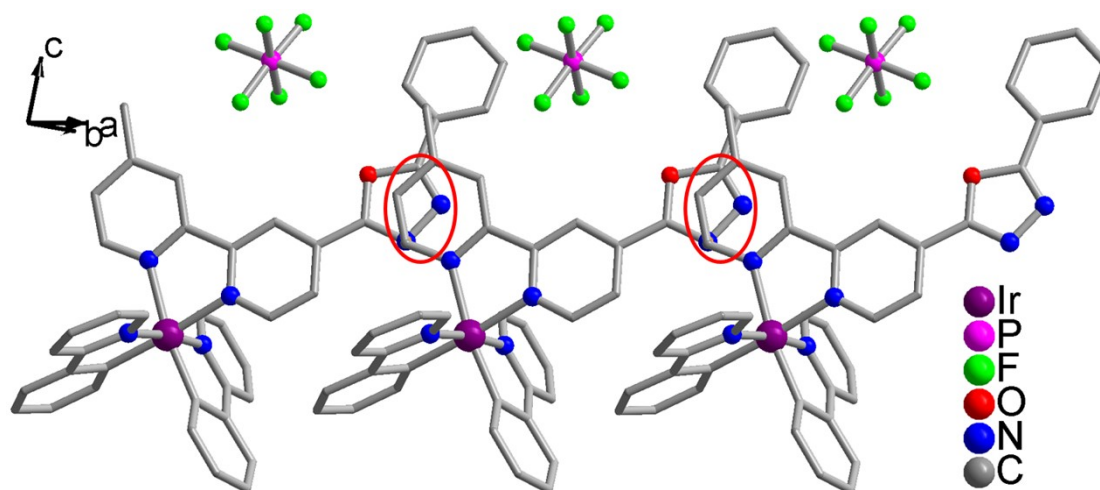


Fig. S6 Top view of the overlapping neighboring $[\text{Ir}(\text{ppy})_2(\text{mbpy-poda})]^+$ cations with $\pi\cdots\pi$ stacking interaction (see red ring part) between pyridine moiety and 1,3,4-oxadiazole unit in complex **1-O**.

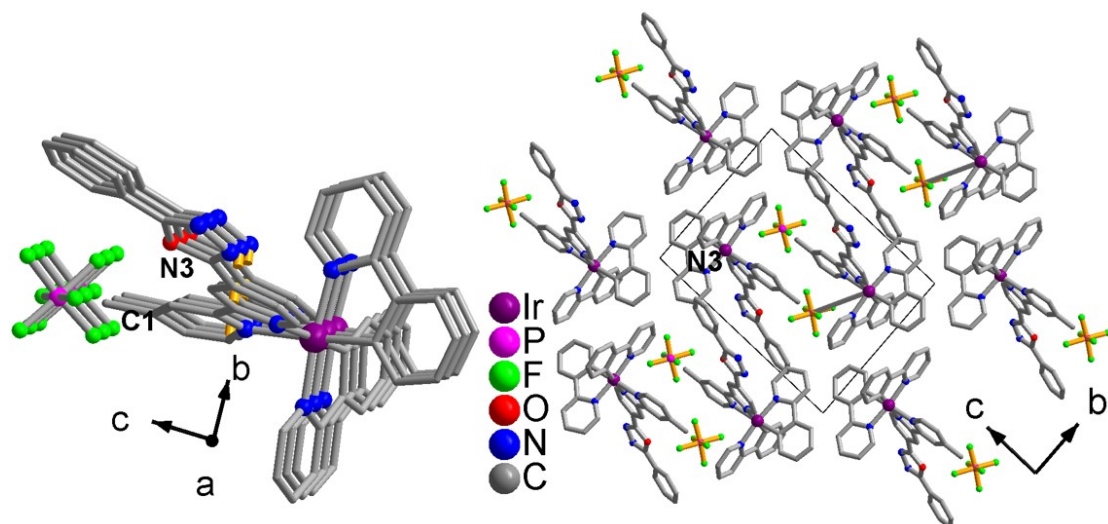


Fig. S7 Supramolecular chain structure (left) and packing structure (right) of 1-O.

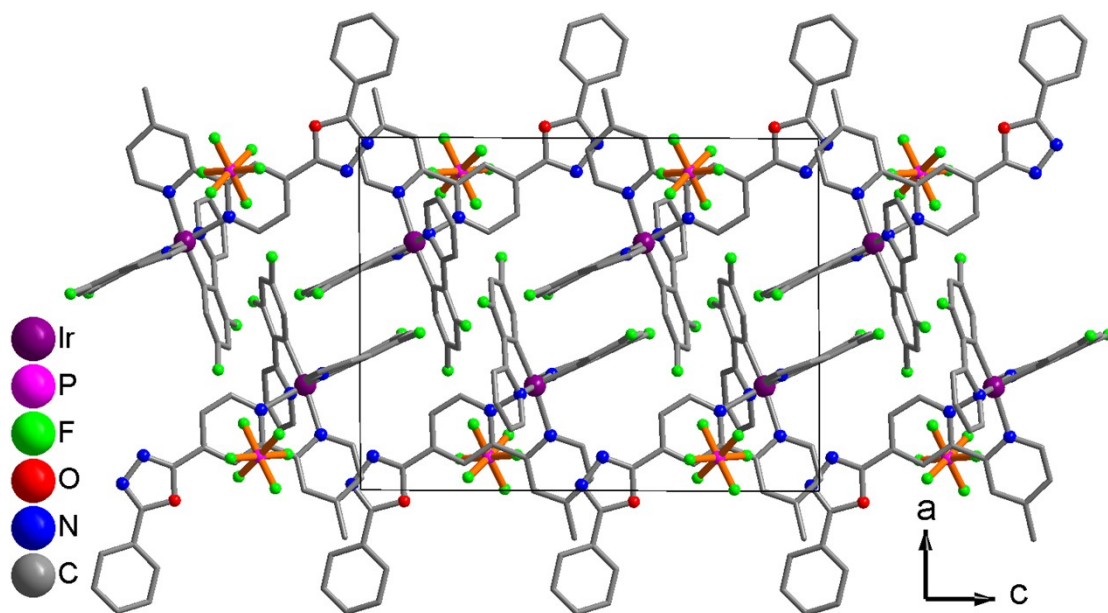


Fig. S8 Packing structure of 2-O.

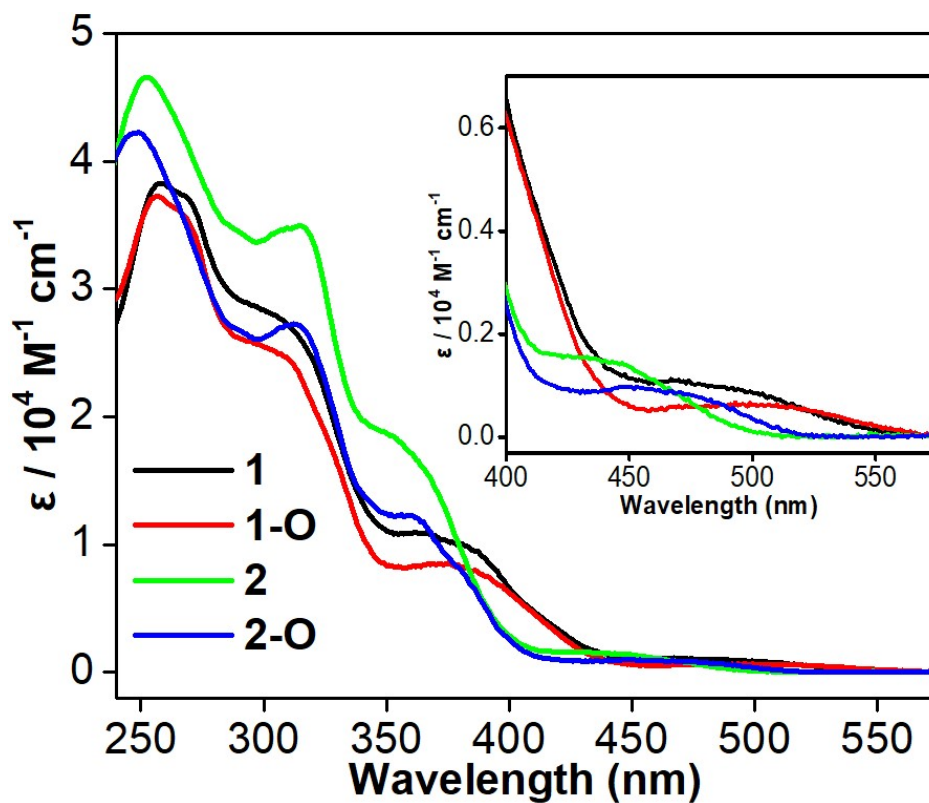


Fig. S9 UV-vis absorption spectra of **1**, **1-O**, **2** and **2-O** in CH_2Cl_2 ($c = 1 \times 10^{-5}$ M) at room temperature.

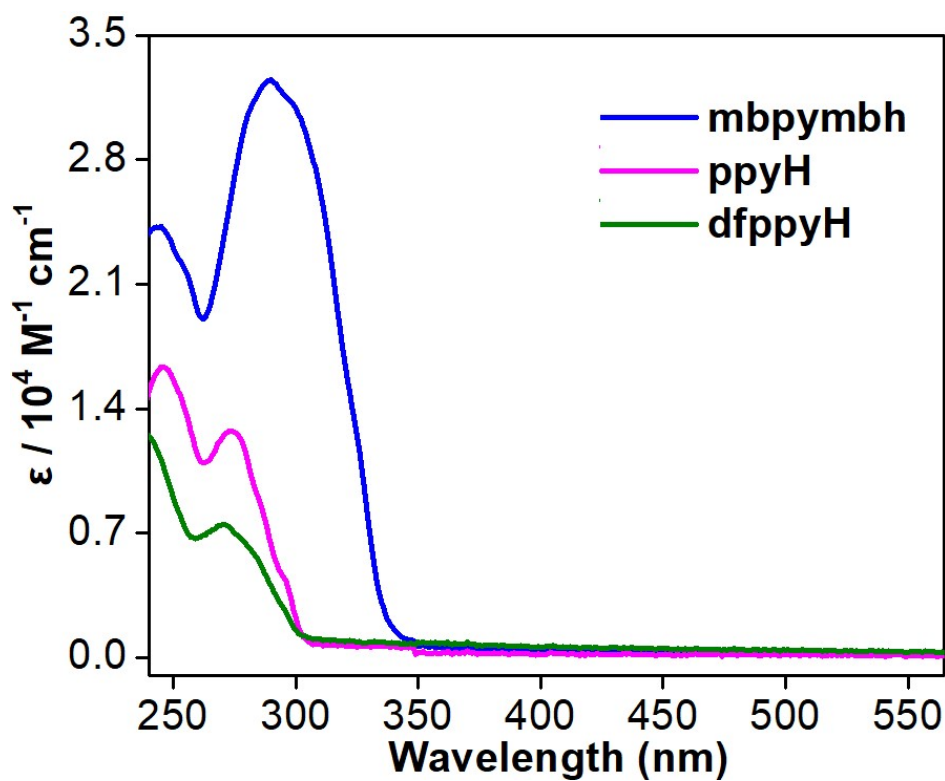


Fig. S10 UV-vis absorption spectra of mbpymbh, ppyH and dfppyH in CH_2Cl_2 ($c = 1 \times 10^{-5}$ M) at room temperature.

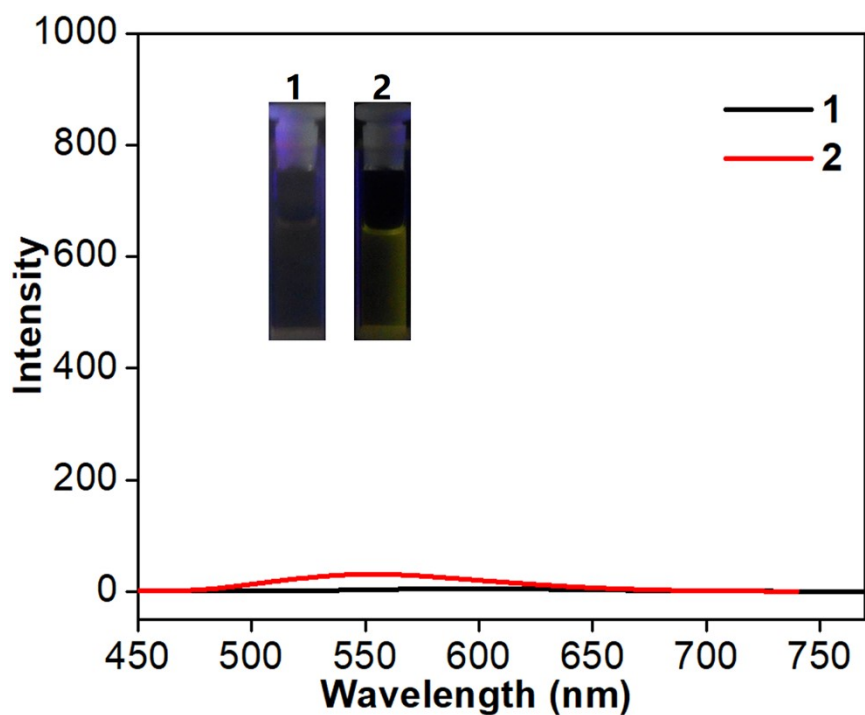


Fig. S11 Luminescence spectra of complexes **1** and **2** ($c = 1 \times 10^{-4}$ M, $\lambda_{\text{ex}} = 370$ nm) in CH_2Cl_2 at room temperature.

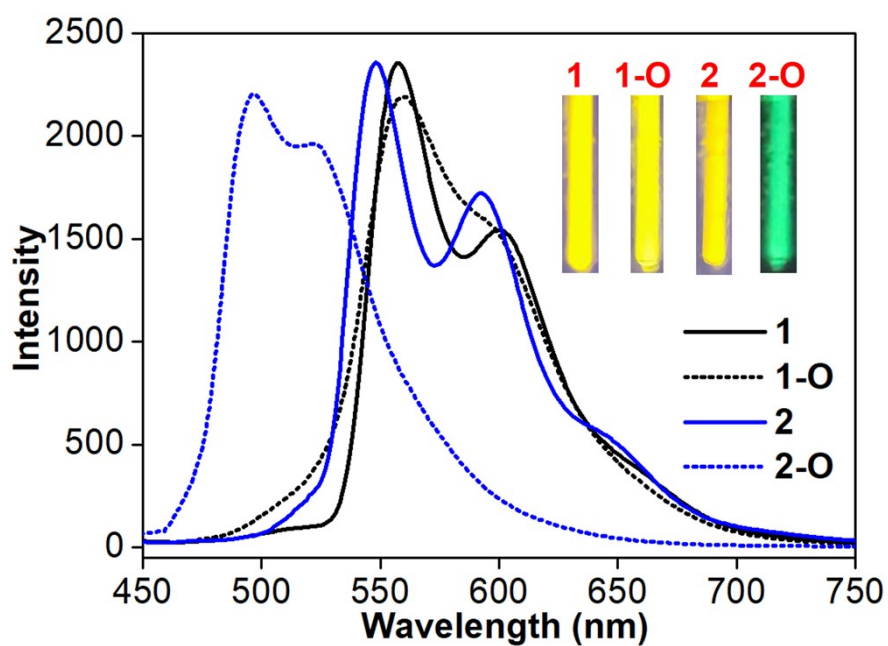


Fig. S12 Luminescence spectra of complexes **1**, **2**, **1-O** and **2-O** in $\text{CH}_3\text{CH}_2\text{OH}-\text{CH}_3\text{OH}$ ($v/v = 3/1$) at 77 K.

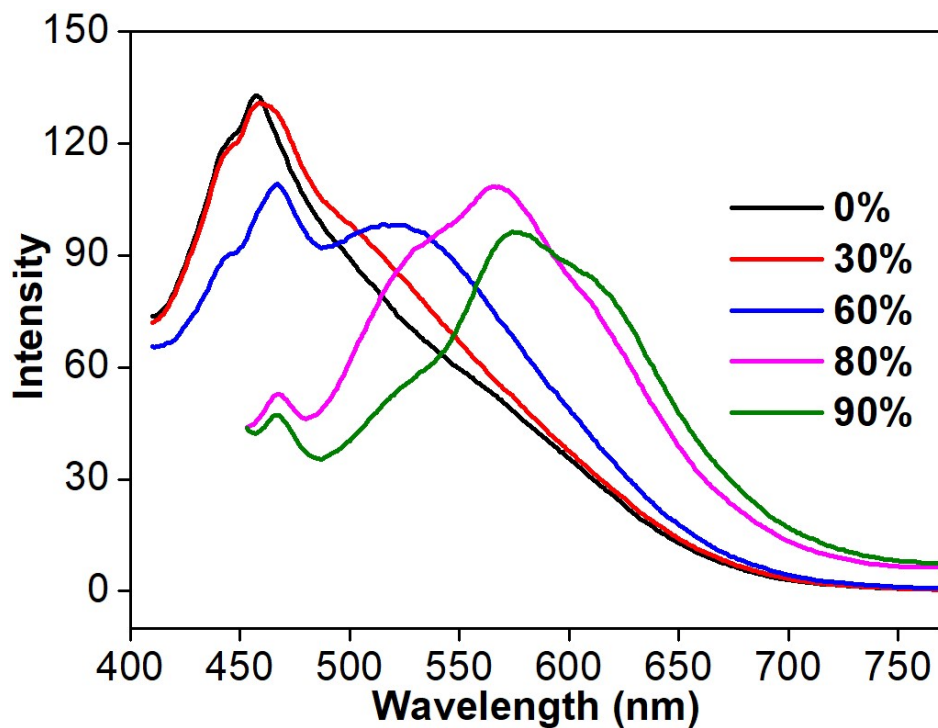


Fig. S13 Luminescence spectra of **2** ($\lambda_{\text{ex}} = 399$ nm) in a CH₃CN-H₂O mixed solvent with different water fractions at room temperature.

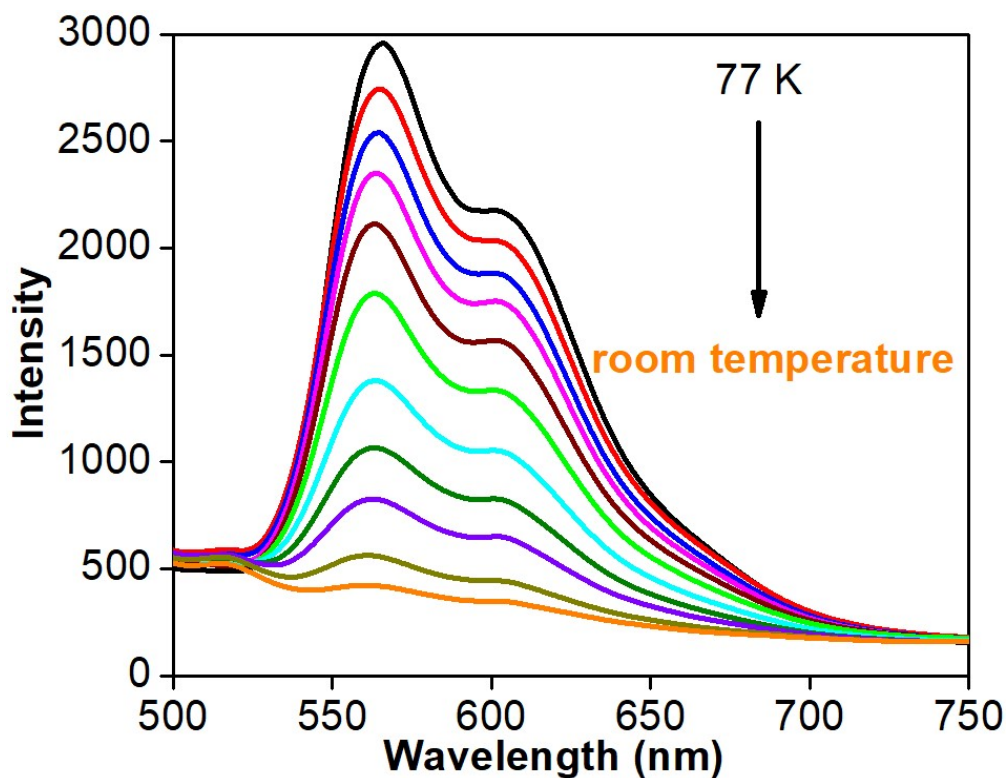


Fig. S14 Luminescence spectra changes of **2** ($\lambda_{\text{ex}} = 399$ nm) in a CH₃CN-H₂O (v/v = 1:9) mixed solvent upon increasing temperature from 77 K to room temperature.

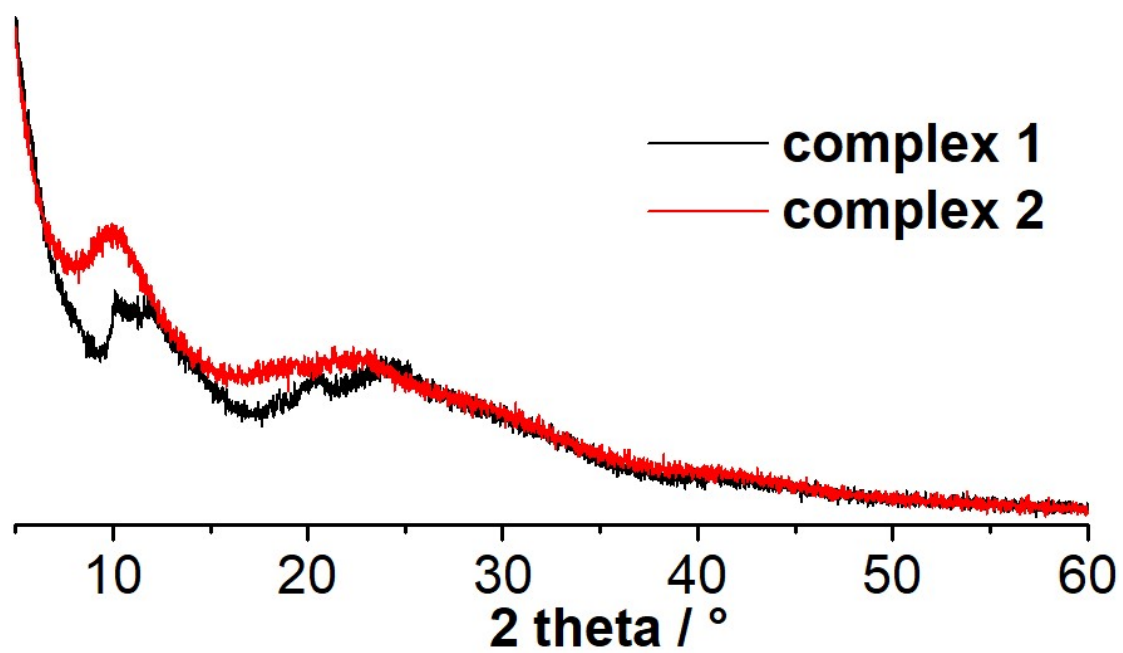


Fig. S15 Experimental XRD patterns of aggregates formed by complexes 1 and 2.

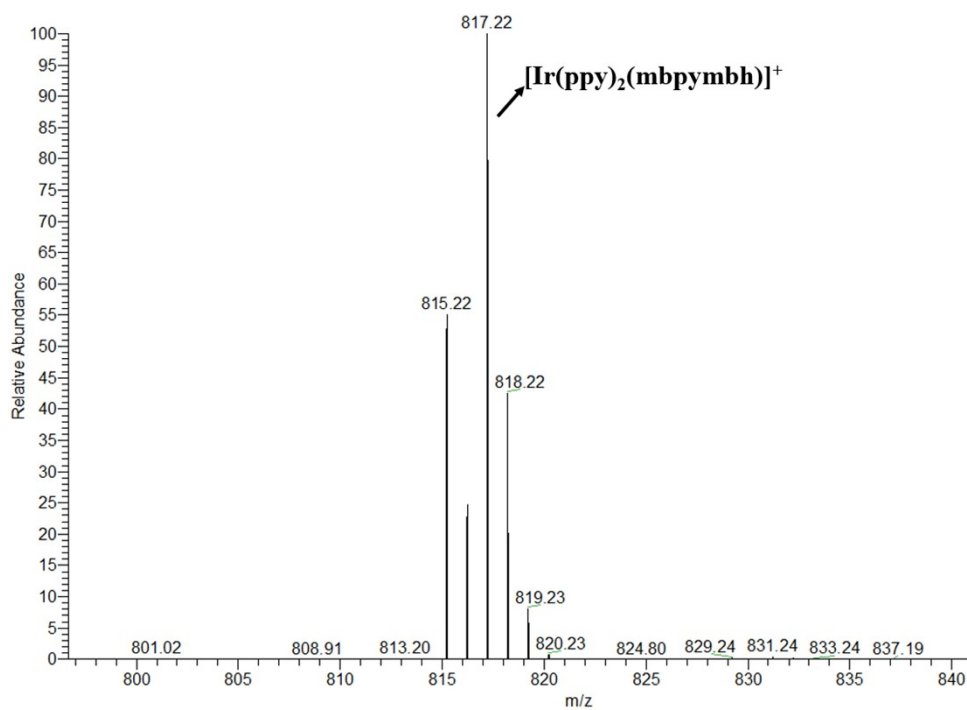


Fig. S16 ES mass spectrometry of complex 1.

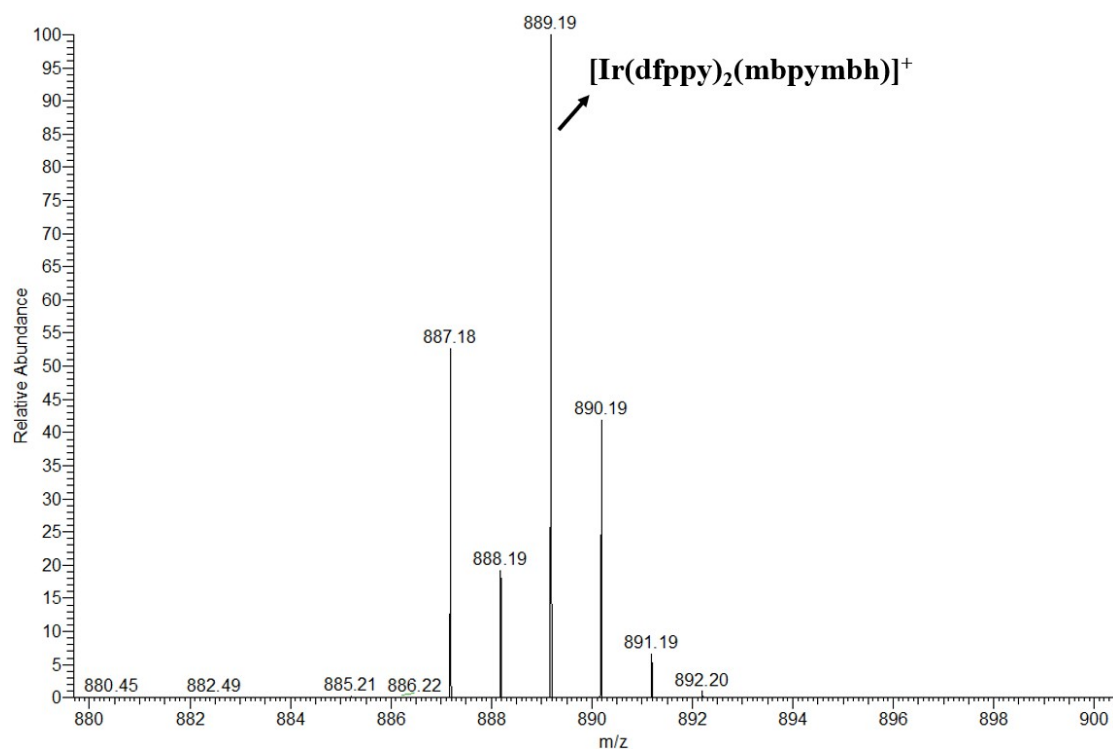


Fig. S17 ES mass spectrometry of complex 2.

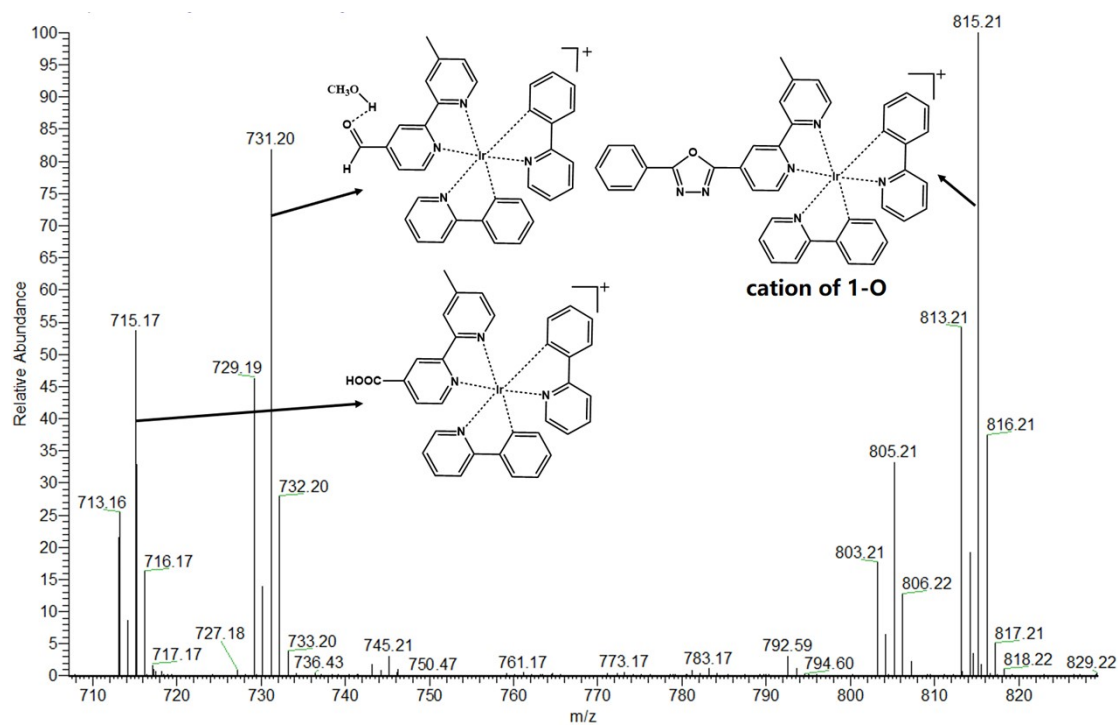


Fig. S18 ES mass spectrometry of complex 1 after irradiation with 365 nm light

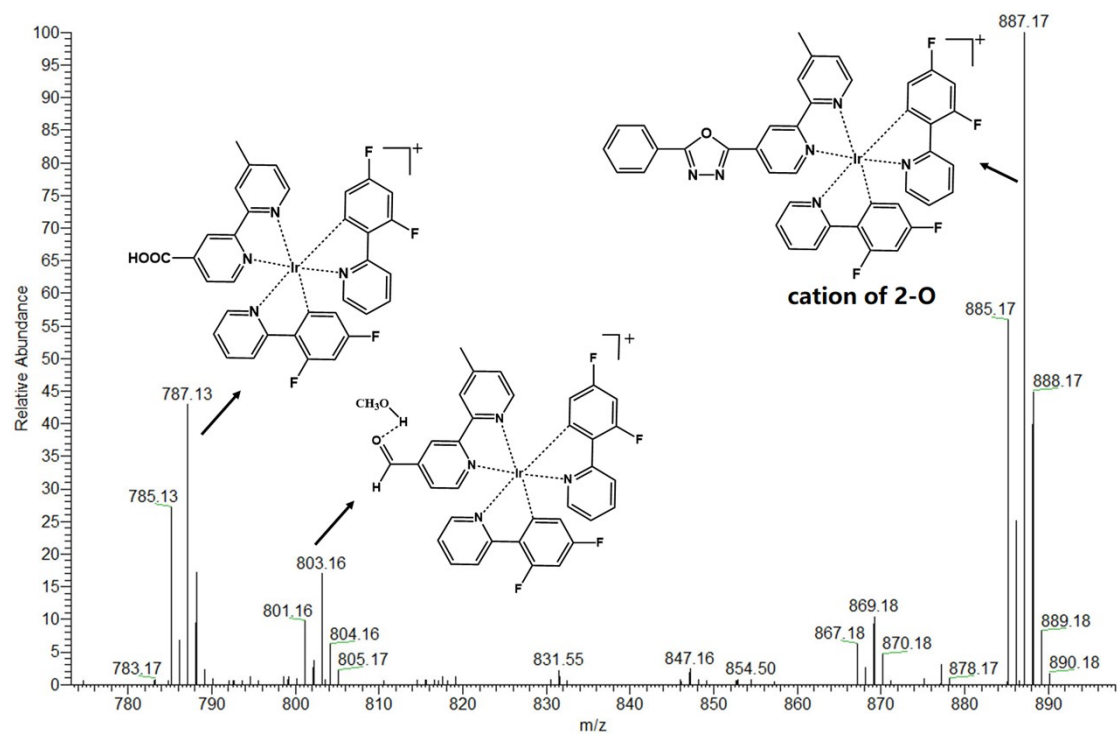


Fig. S19 ES mass spectrometry of complex **2** after irradiation with 365 nm light.

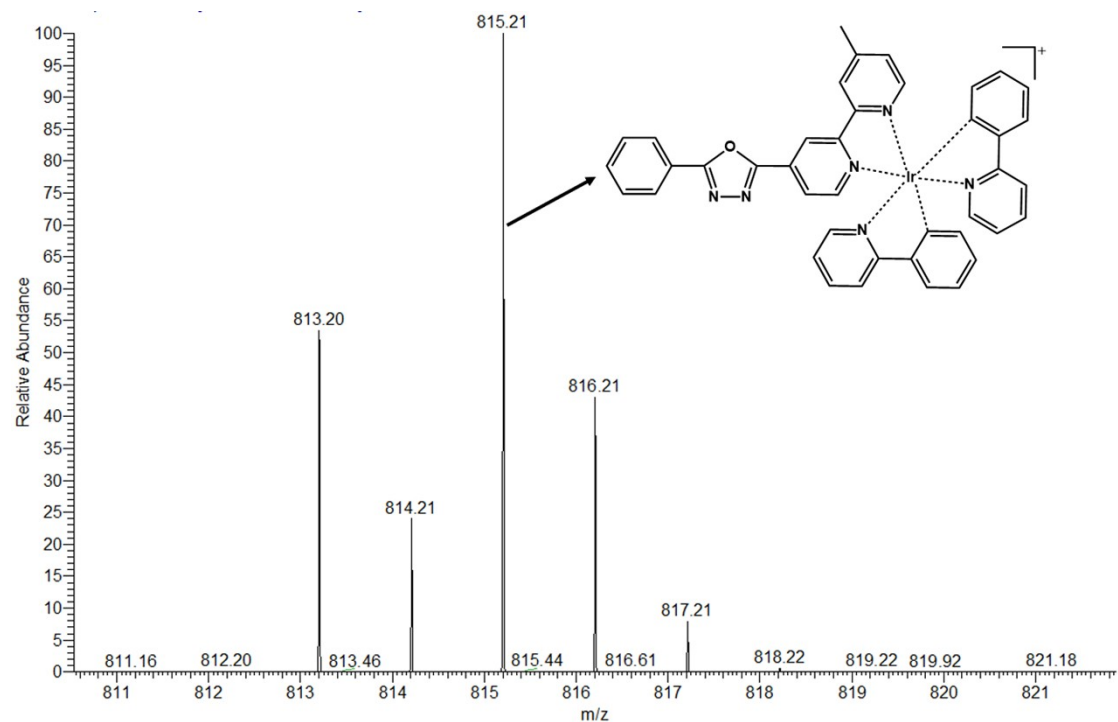


Fig. S20 ES mass spectrometry of complex **1-O**.

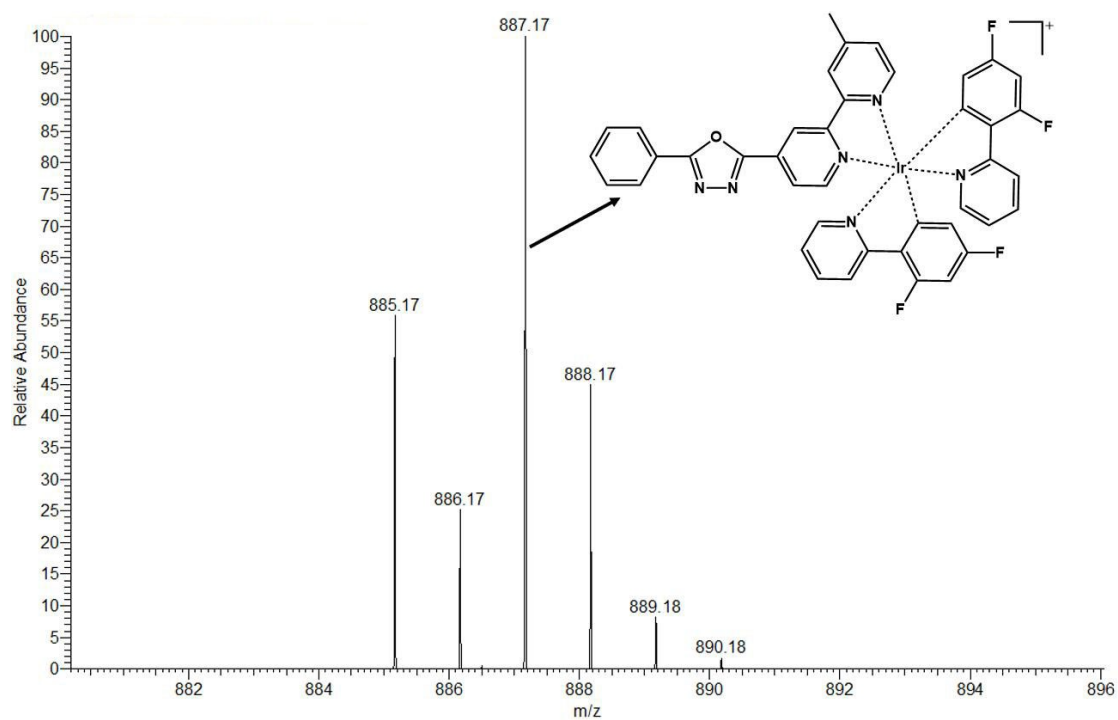


Fig. S21 ES mass spectrometry of complex 2-O.

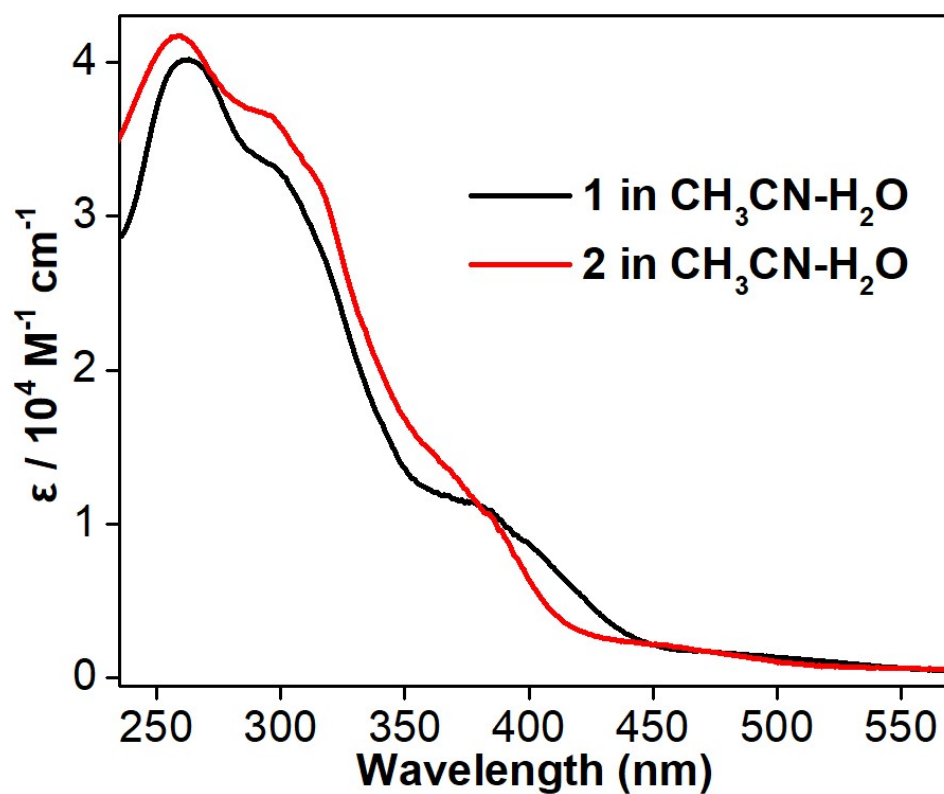


Fig. S22 UV-vis absorption spectra of 1 and 2 ($c = 1 \times 10^{-5} \text{ M}$) in $\text{CH}_3\text{CN-H}_2\text{O}$ (v/v = 1/9) at room temperature.

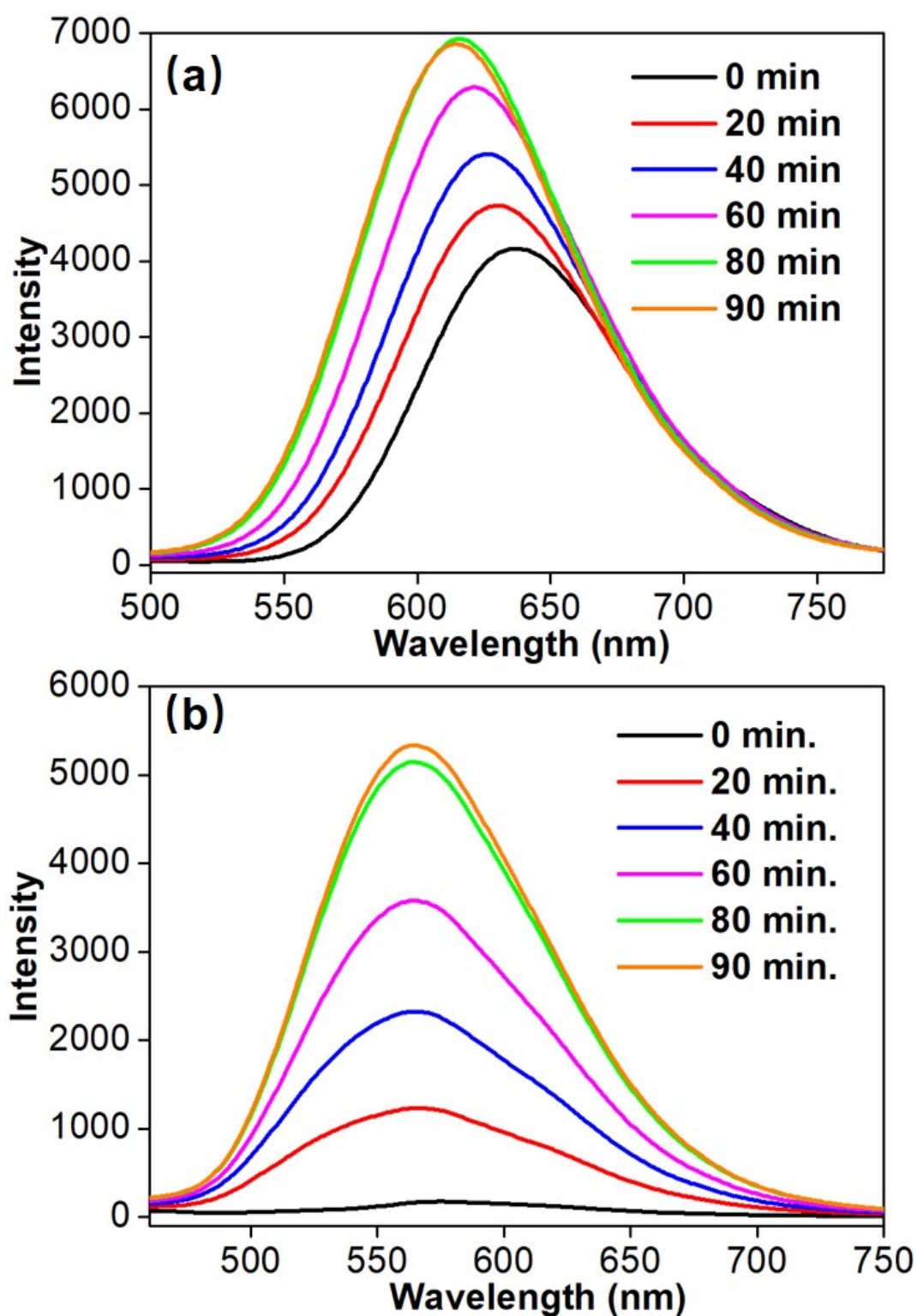


Fig. S23 Luminescence spectra changes of **1** (a) and **2** (b) in CH₃CN-H₂O (v/v = 1/9) mixed solvent ($c = 1 \times 10^{-4}$ M, $\lambda_{\text{ex}} = 399$ nm) upon irradiation with 400 nm light.

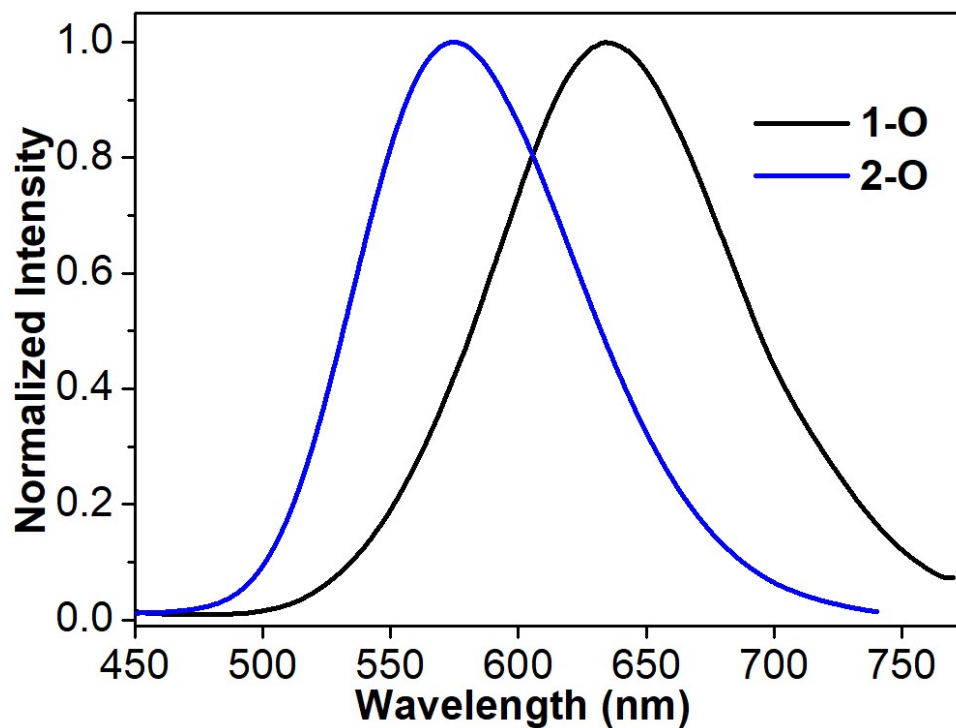


Fig. S24 Luminescence spectra of complexes **1-O** and **2-O** in CH_3CN ($c = 1 \times 10^{-4} \text{ M}$, $\lambda_{\text{ex}} = 385 \text{ nm}$ for **1-O** and 370 nm for **2-O**).

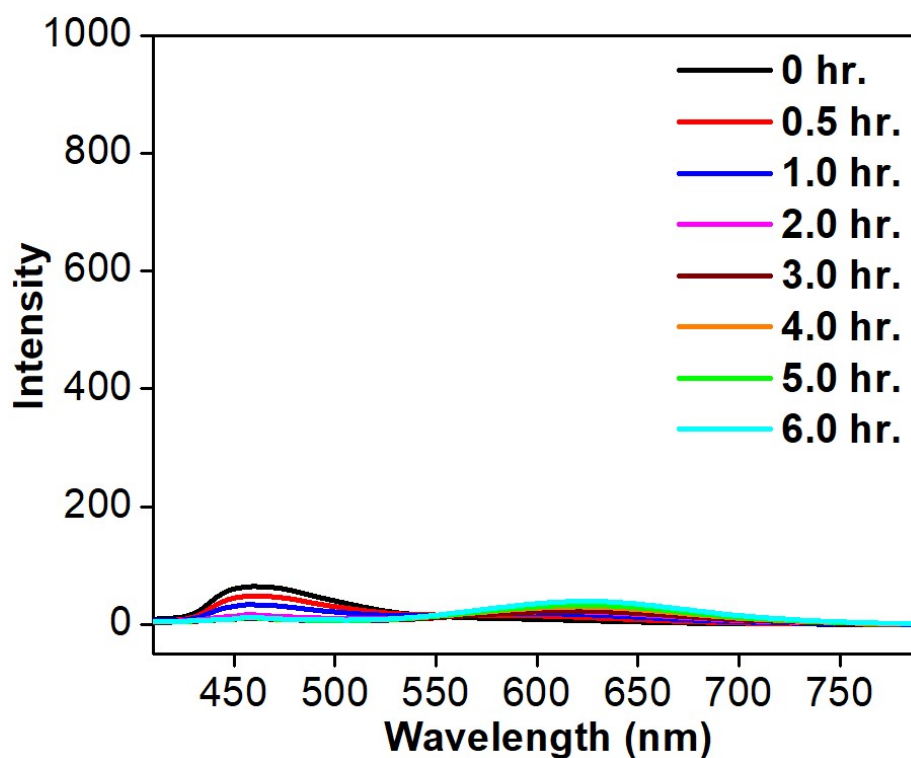


Fig. S25 Luminescence spectra changes of complex **1** in CH_3CN upon irradiation with 365 nm light ($c = 1 \times 10^{-4} \text{ M}$, $\lambda_{\text{ex}} = 399 \text{ nm}$).

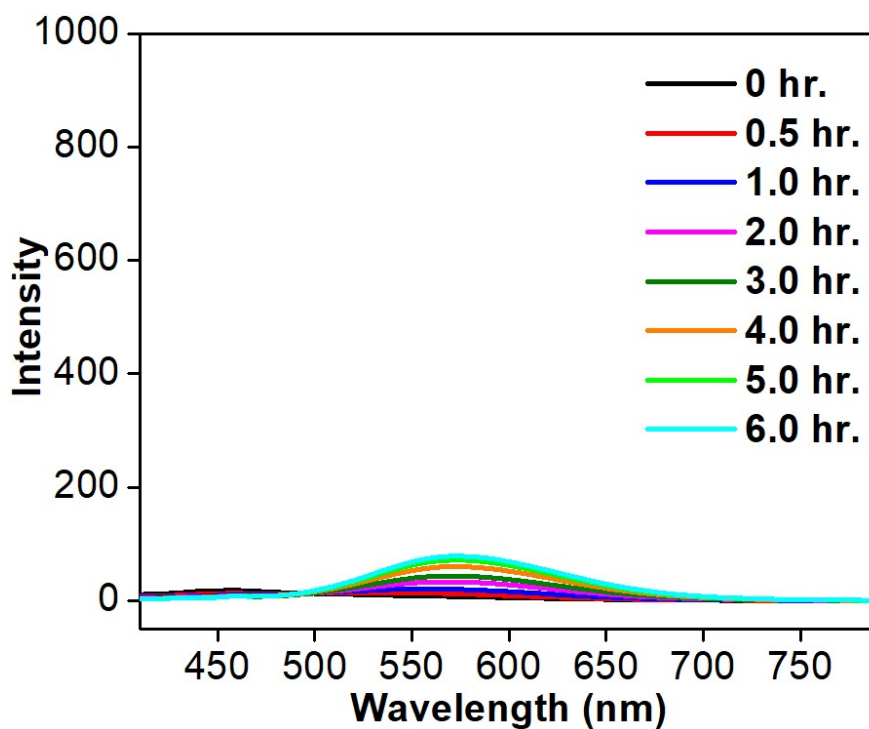


Fig. S26 Luminescence spectra changes of complex **2** in CH₃CN upon irradiation with 365 nm light ($c = 1 \times 10^{-4}$ M, $\lambda_{\text{ex}} = 399$ nm).

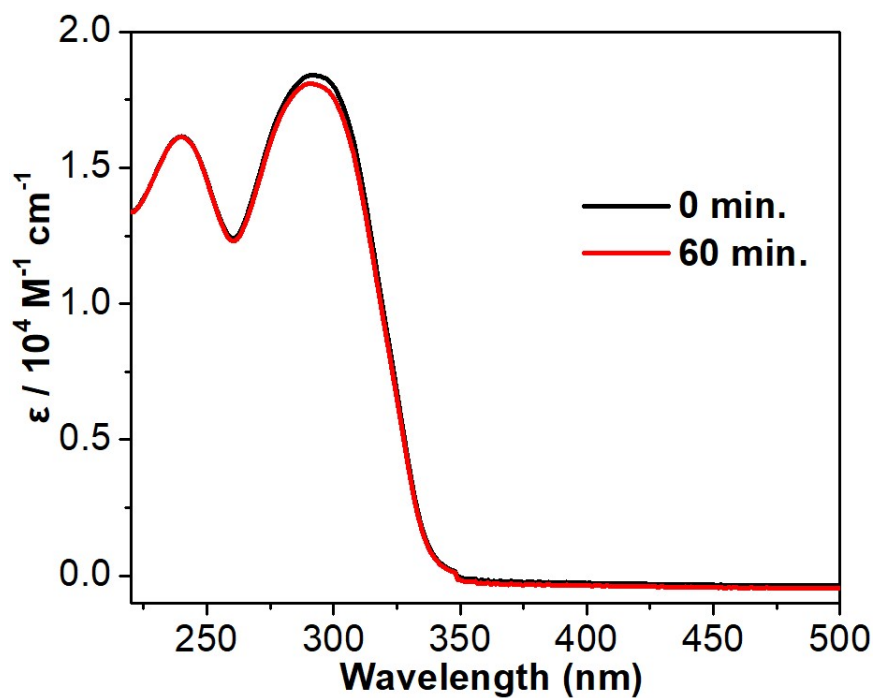


Fig. S27 UV-vis absorption spectra of ligand mbpymbh ($c = 1 \times 10^{-5}$ M) in CH₃CN-H₂O ($v/v = 1/9$) before irradiation and after irradiation with 365 nm light for 60 minutes at room temperature.

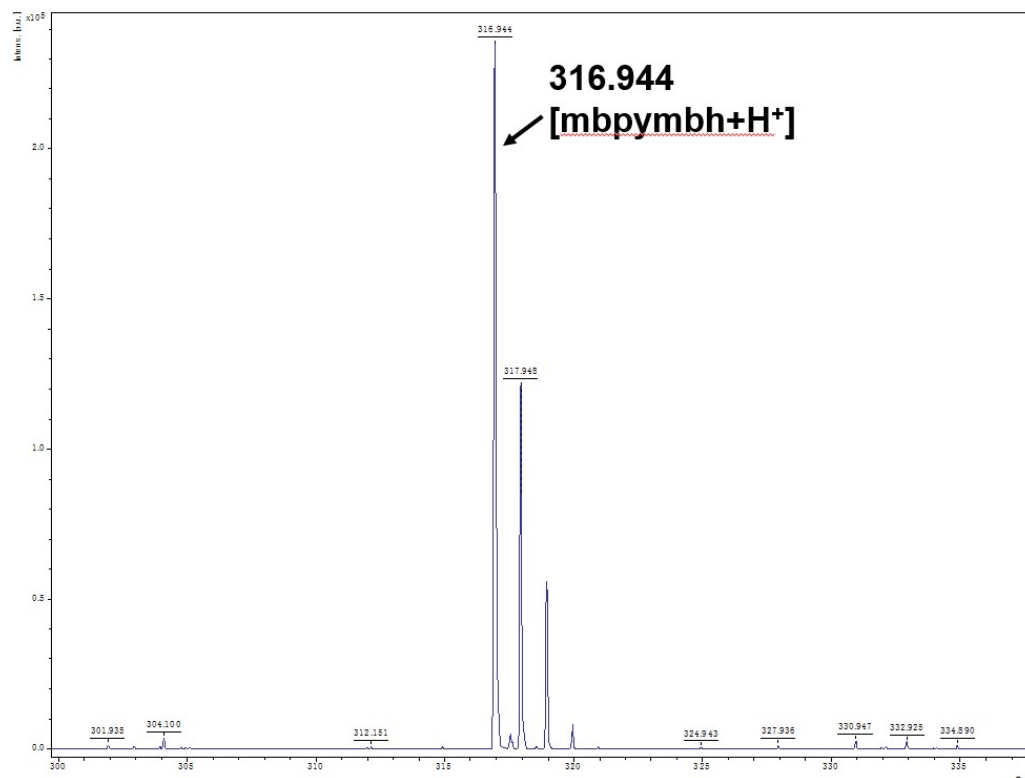


Fig. S28 MALDI-TOF spectrum of mbpymbh after irradiations with a light source (wavelength range: 310-400 nm) for sixty minutes in a CH₃CN-H₂O (v/v =1/9) mixed solvent.

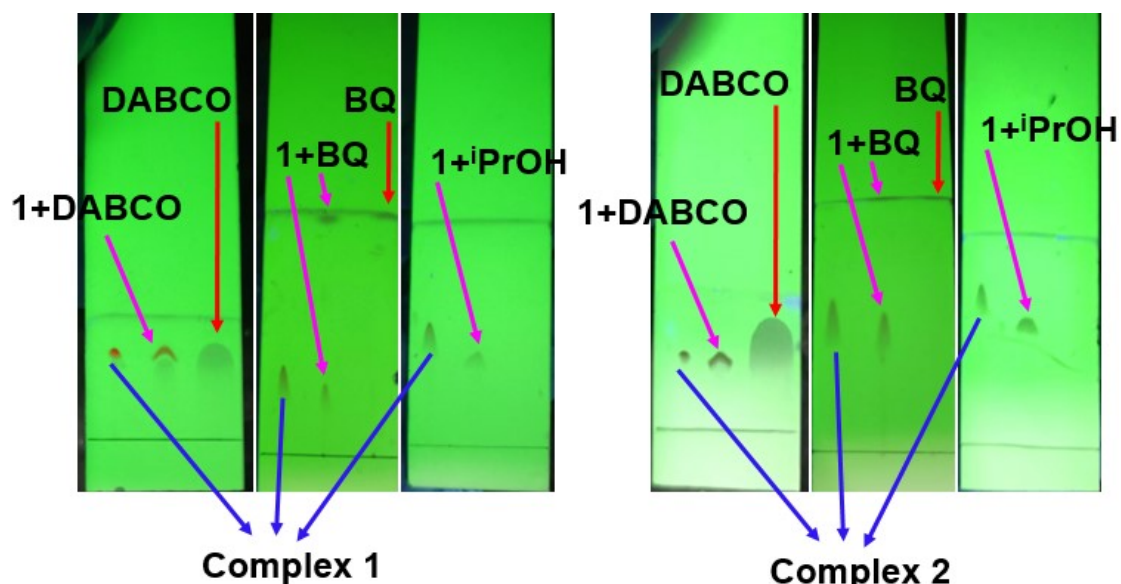


Fig. S29 Thin layer chromatography (TLC) analyses of mixtures containing aggregates of complex 1 (or 2) with scavengers (DABCO, BQ and ⁱPrOH), and control samples (1, 2 and ⁱPrOH alone). Development in CH₂Cl₂/MeOH (v/v =30/1). Photographs were taken under 254 nm UV light.

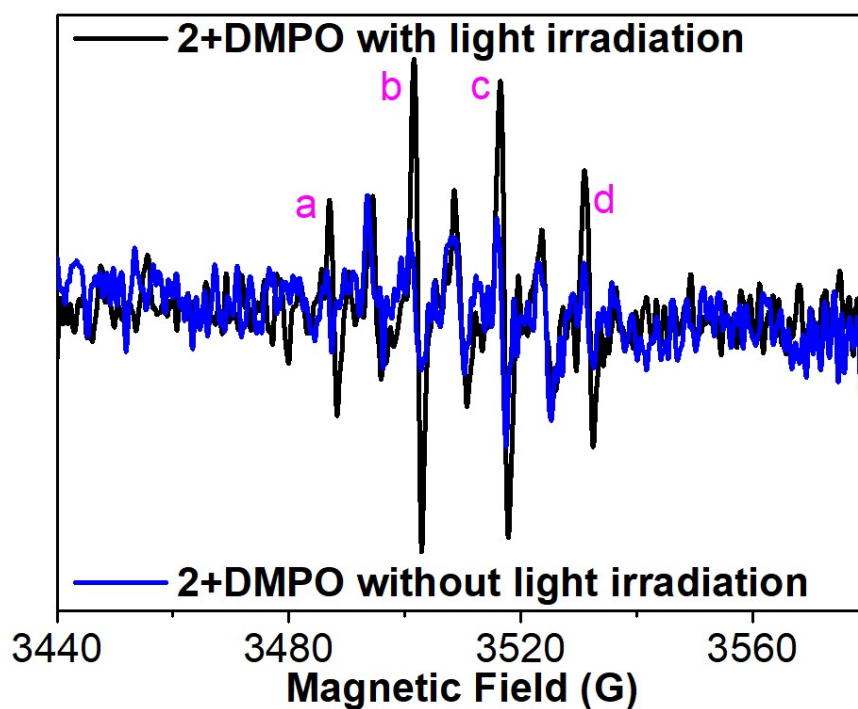


Fig. S30 EPR spectra of 2-DMPO mixture in a $\text{CH}_3\text{CN-H}_2\text{O}$ ($v/v=1/9$) mixed solvent with irradiation with 365 nm light (black plot), and without light irradiation (blue plot).

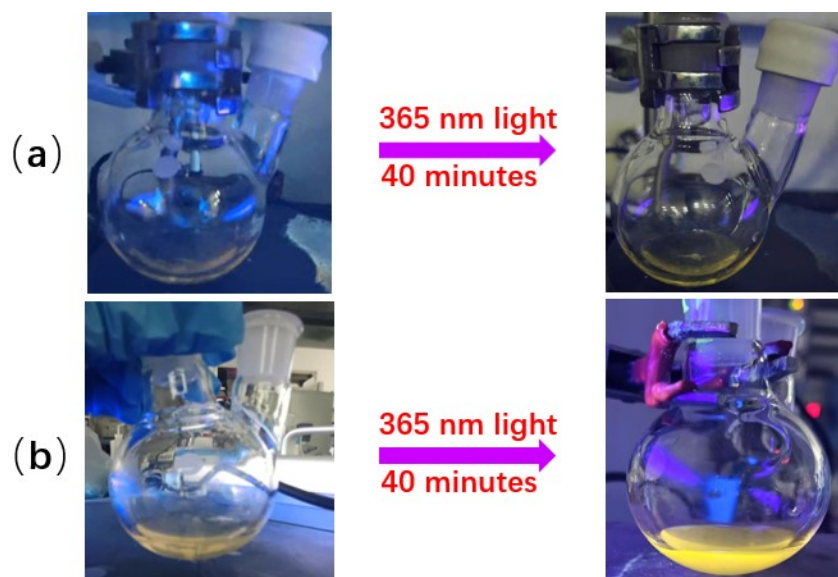


Fig. S31 Luminescence changes of complex 2 in $\text{CH}_3\text{CN-H}_2\text{O}$ ($v/v = 1/9$) upon irradiation with 365 nm light for 40 minutes under argon (a) and under air (b).